Effect of carbon black properties on cut and chip wear of natural rubber

William Amoako Kyei-Manu [a], Lewis B. Tunnicliffe [b], Charles R. Herd [b], Keizo Akutagawa [a], Radek Stoček [c,d], James J.C. Busfield [a,*]

[a] School of Engineering and Materials Science, Queen Mary University of London, London, E1 4NS, United Kingdom
[b] Birla Carbon, Marietta, GA, 30062, USA
[c] Centre of Polymer Systems, Tomas Bata University in Zlín, Zlín, Czech Republic
[d] PRL Polymer Research Lab, Zlín, Czech Republic

ARTICLE INFO

ABSTRACT

The effect of carbon black colloidal properties on cut and chip wear of natural rubber compounds is investigated across a wide range of applied impact normal forces using an Instrumented Cut and Chip Analyzer (ICCA). The objective of the study is to determine the basic fatigue and fracture mechanisms that drive cut and chip wear. Natural rubber compounds reinforced with eight different carbon blacks varying in structure and surface area are studied. The loading of the carbon blacks in the rubber compounds is fixed at 50 parts per hundred rubber (phr). The cut and chip performance strongly correlates to both the carbon black morphological properties and the resulting compound mechanical and fracture properties. The cut and chip performance also depends on the applied impact normal force level. At low forces, high structure carbon blacks result in compounds which are stiffer and deflect less under the applied impact normal forces and minimize cut and chip wear. At high forces, low structure carbon black compounds, which are softer and more readily able to crystallize under force-controlled deflection, minimize cut and chip wear. It is argued that at low applied impact normal forces, the cut and chip behavior is dominated by a force-controlled fatigue crack growth mechanism which transitions to a critical tearing energy dominated mechanism at high applied impact normal forces. It is therefore important to understand the severity of application to select optimum compound properties such as the carbon black type to minimize cut and chip wear in application.

1. Introduction

Cut and chip, fatigue and abrasive wear are the principal causes of tire tread damage which lead to replacement of tires. While the more familiar fatigue and abrasive wear typically occur in tires used in long haul, regional and urban roads [1], cut and chip wear is an in-service failure mode most commonly seen for truck, bus and radial (TBR) and off-the-road (OTR) tires used on aggressive surfaces and under high loading conditions [2]. Cut and chip wear can also be the dominant type of wear in passenger car tires that are operated consistently on unpaved roads. The size of wear debris particles typically increases from nanometers to centimeters in magnitude from fatigue to abrasive and then to cut and chip wear.

Cut and chip wear as the name suggests, is a two-step in-service failure process. Beatty and Miksch [3] provided the first formal definition of cut and chip. "Cutting occurs rapidly when a sharp object such as a rock strikes a tire tread with enough force to penetrate the tread compound. Chipping usually occurs after a cut because of forces imparted on the tire tread during braking, turning or from other tractive forces from driving on rough or sharp surfaces. Chipping causes tearing of the rubber normally at 90° to the direction of the cut. Chipping can also occur as a first step if there is relative motion between the tire tread and a sharp object." Chunking, which refers to the tearing away of large chips can also occur [4]. Chipping and chunking cause pieces of rubber tread to be removed which makes the tire more susceptible to failure. Cut and chip wear can also be observed on rubber tracks or conveyor belts [5] where large sharp rocks are dropped on the moving belt.

Tires prone to cut and chip wear include those on giant earthmoving vehicles like mining dump trucks and those on vehicles used for agricultural operations. The tires on these vehicles can be large with diameters of several meters [6] and they move at relatively slow speeds across high severity surfaces. Changing these large tires due to failures such as cut and chip wear can be time-consuming, costly and can pose safety hazards. It is therefore critical to study and understand the

---

* Corresponding author.

E-mail address: j.busfield@qmul.ac.uk (J.J.C. Busfield).

complex cut and chip phenomenon to minimize its occurrence in the field.

Cut and chip wear testing has been performed in the field for scientific research. Some experiments [3,4,7–10] showed similar cut and chip resistance ranking to comparable materials tested in the laboratory while a few [11] did not show correlation between the field and laboratory tests. Performing cut and chip wear testing in the field can be costly and it is also difficult to perform controlled, repeatable tests. There is a need therefore for laboratory tests that closely replicate in-service conditions to understand cut and chip wear.

Beatty and Miksch [3] performed the first recorded laboratory cut and chip experiments that showed the same performance ranking as materials from field testing. They estimated the cut and chip wear from the change in diameter of a wheel measuring approximately 50.8 mm in diameter and 12.7 mm in width rotated at a rotational speed of 750 rpm and impacted with a metallic indenter using a force of ~12.59 N. Subsequent experiments have discussed how properties such as crosslink density [12–14], energy dissipation [3,9,15–18], modulus [3,12], and elongation at break [3,12] may influence cut and chip wear. However, there is conflicting information on how some of these properties affect cut and chip resistance.

The effects of properties such as critical tearing energy and fatigue crack growth on cut and chip resistance is also still widely debated. Some researchers have attributed an increase in cut and chip resistance with increasing critical tearing energy [3,7,15,19]. Beatty and Miksch [3] however reported no correlation of cut and chip resistance with critical tearing energy from testing carbon black reinforced styrene butadiene rubber compounds. They however observed a correlation between critical tearing energy and cut and chip resistance in a set of carbon black reinforced natural rubber compounds and attributed this to the wider range of compounds tested. Ahmad et al. [4] argued that cutting is unrelated to critical tearing energy, but chipping of rubber material is critical tearing energy dependent.

Ahmad et al. [4] also argued that neither cutting nor chipping is related to crack propagation since crack propagation is a fatigue property. Stoček et al. [17,20] however showed that while fatigue crack growth had no quantitative predictive value on cut and chip resistance, there was a qualitative correlation with tests showing that the ranking of cut and chip resistance followed the same ranking of fatigue crack growth resistance of tested rubber compounds [17]. Using simulation techniques, Robertson et al. [21] showed that at low applied impact normal forces, fatigue life predictions followed the same relative cut and chip resistances of tested butadiene rubber, natural rubber and styrene-butadiene rubber compounds. However, at high applied impact normal forces, impact-induced temperature increases needed to be considered in the fatigue analysis to match the experimental cut and chip resistance ranking. Robertson et al.'s [21] testing provided evidence to support the concept that rubber fracture mechanics dominates the cut and chip phenomenon leading them to coin the term, "crack and chip" to reflect the mechanisms involved in the cut and chip wear accumulation process.

A complete and fully accepted understanding of cut and chip wear as it relates to fatigue and fracture behaviour has yet to be realized. Although cut and chip resistance in rubber materials may seem well-researched, a recent Web of Science search revealed fewer than 50 articles on the topic—less than 3 % in comparison to the over 2000 articles published on fatigue and abrasive wear in rubber materials. When experimental research is conducted, it normally also focuses on a narrow range of applied impact normal forces which makes it difficult to draw conclusions about field applications and may also explain some of the reported conflicting effects on cut and chip wear. It is also important to note that while research has been performed on the effect of particulate reinforcements such as silica [15,16,22], aramid fibers [15,23], nano-dispersed clay [24] and rice husk silica [25] on cut and chip wear, very little research has been performed on the effect of carbon black, which is the most widely used particulate reinforcement in the tire

industry.

The objective of this work is to understand the underlying mechanisms of cut and chip wear. This is achieved by performing a comprehensive and systematic study on the influence of carbon black's colloidal properties, specifically surface area and structure, on the cut and chip resistance of natural rubber. An Instrumented Cut and Chip Analyzer allows field conditions to be better replicated - including testing a broad range of applied impact normal forces. A wide colloidal space of furnace carbon blacks varying only in their structure and surface area was evaluated. The wide variety of carbon blacks coupled with the wide range of tested applied impact normal forces allow statistical interpolation of the cut and chip results. From the results, new correlations with material properties and insights into the origins of cut and chip wear, as it relates to fatigue and fracture properties, can be drawn. Consequently, selection guides to minimize cut and chip wear using carbon blacks are provided.

1.1. Carbon black

Carbon black is the most widely used reinforcing particulate in tires and the rubber industry in general. It is comprised of >95 % elemental carbon with the fundamental particulate unit being the aggregate which is a fused assembly of spherical para-crystalline primary particles with diameters ranging from ~5 nm to ~200 nm [26]. Carbon black is made from the controlled combustion of hydrocarbon feed stocks typically in furnace reactors [26]. The parameters of the manufacturing process can be controlled to determine the structure, primary particle size and other properties of the resulting carbon blacks. Carbon black surface area and structure influence properties of rubber compounds including the static and dynamic mechanical properties [27,28], fatigue crack growth resistance [29], abrasion resistance [30], temperature rise [31], heat build-up [32] and degree of crystallization upon stretching [33].

The primary particle size is the most basic building block before surface and aggregate growth lead to the formation of aggregates. Particle size can be measured directly using transmission electron microscopy [34] or inferred from surface area measurements through gas adsorption techniques [35]. Primary particle size has an inverse relationship with the surface area per unit mass of carbon black [26]. Structure refers to the number and spatial arrangement of the primary particles comprising the aggregate. Structure is typically measured using oil absorption techniques [36,37].

Particle size and structure are important in determining the enhancement of properties imparted to rubber compounds by carbon black. The primary particle size defines the contact area between carbon black and rubber and the number of aggregates per unit volume of rubber. The primary particle size therefore governs the average inter-aggregate distance and aggregate-aggregate networking which influences properties such as energy dissipation in the rubber material. The structure affects the reinforcement in the rubber since it determines the volume of rubber occluded from globally applied strains by aggregate branches. The effective volume fraction of carbon black in the rubber is the sum of the volume of carbon black and the volume of occluded rubber, and directly impacts the level of strain amplification [38].

Other important properties of carbon black include the surface activity, porosity, aggregate size distribution and thermal history. However, a detailed exploration of the effects these properties have on cut and chip wear is beyond the scope of this current study.

1.2. Instrumented Cut and Chip Analyzer

The cut and chip wear tests were performed using an Instrumented Cut and Chip Analyzer (ICCA). The ICCA was recently developed by Coesfeld GmbH & Co. KG, Germany and is now used in industry for cut and chip wear testing. It is a multichannel instrument where a rubber wheel is rotated and impacted with a stainless-steel indenter at a

specified frequency. The metallic nature of the indenter results in inherently different thermal conductivity and frictional properties compared to an actual road surface. The impact is produced using a pneumatic cylinder where the applied impact normal force, frequency, and contact time with the rubber surface can be independently controlled. Fig. 1 shows an image of the ICCA and a chamber where the test is conducted.

The rubber wheel specimen for the ICCA has outer and inner diameters of 55 mm and 26 mm respectively, and a thickness of 13 mm. The inner surface of the specimen is gear shaped to allow for a strong connection to the rotational drive and this prevents the specimen from slipping during testing. A schematic and photograph of the ICCA rubber test specimen is shown in Fig. S1 in supplementary information. The width of the indenter is about 6.35 mm, and the tip is semi-circular shaped with a radius of 2.5 mm.

Table 1 shows the ICCA parameters and their corresponding ranges that can be pre-defined and controlled by the user. The table also shows proposed test conditions to replicate a specific target application as discussed in the supplementary information.

In addition to the controlled parameters shown in the table, the ICCA can measure parameters such as the shear force, depth of indentation and temperature of the sample surface. Other parameters such as the normal and frictional energies and friction coefficient can be calculated thus allowing more information to be gleaned from the cut and chip wear testing. The ICCA also calculates a cut and chip wear factor, P, which is used to measure the cut and chip damage.

1.2.1. Cut and chip wear factor, P

The ICCA characterizes the cut and chip wear using a cut and chip wear factor, P. The determination of P is performed in situ. P therefore can be obtained during a test and does not require the test to be stopped versus determining cut and chip wear from mass or diameter measurements where the test needs to be stopped to measure the mass and diameter at a given cycle number.

The cut and chip wear factor reflects the specimen surface roughness or damage. The cut and chip wear factor is calculated from incremental changes to the measured range of the shear forces over several impact cycles. When the indenter impacts the rubber specimen at a given applied impact normal force, a shear force is generated across the time of contact as shown in Fig. S2 in supplementary information.

Fig. 2 shows the variation in shear force up to 7000 cycles and highlights the maximum and minimum shear forces in blue and red respectively. The cut and chip wear factor, P, at a specific cycle is typically calculated over the previous 10 cycles.

The cut and chip wear factor, P, is determined by integrating the fluctuations in shear force over several cycles using equation (1) where x is the number of cycles.

$$P = \frac{\int_{x=500}^{x} shear\ force\ (max.)dx - \int_{x=500}^{x} shear\ force\ (min.)dx}{x} \quad (1)$$

A higher value of P indicates higher cut and chip wear accrual. Fig. 3

Table 1
Cut and chip wear test parameters and range.

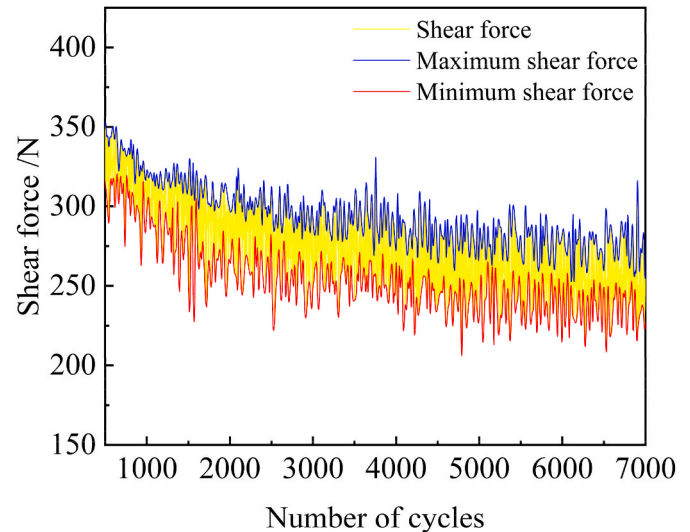| Parameter	Range	Proposed test conditions to replicate specific target application
Applied impact normal force/N	30 to 500	Minimum 90
Rotational speed/rpm	0 to 1500	90
Impact frequency/Hz	0 to 10	1.5
Number of impact cycles	0 to undefined	Varied
Time of contact/ms	30 to permanent	50

Fig. 2. Fluctuation in shear force up to 7000 cycles highlighting maximum and minimum shear forces.

shows the cut and chip wear factor for two wheels. The wheel with greater surface roughness variation (highlighted with the red box) has a higher cut and chip wear factor, while the wheel with less surface roughness variation (highlighted by the blue box) has a lower cut and chip wear factor.

2. Materials and methods

2.1. Materials

Eight different compounds of SMR CV60 natural rubber, each reinforced with a different carbon black grade at 50 parts per hundred (phr) loading, were used for the experiments. The carbon blacks were selected to cover a wide range of surface area and structure as shown by the colored symbols in Fig. 4. The open grey circles highlight some common
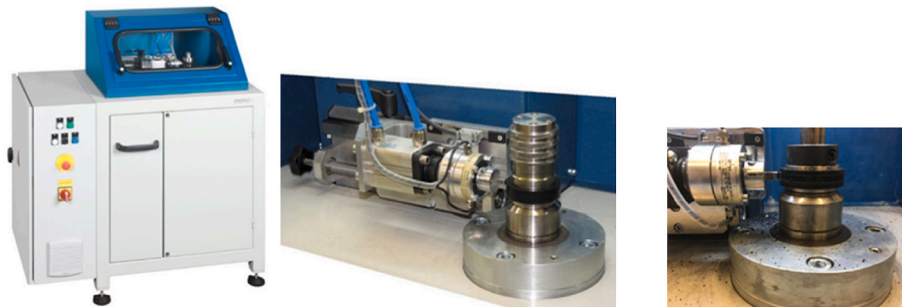

Fig. 1. A photograph of the ICCA (left), a detailed view into the chamber (middle) and a zoomed section showing the rubber wheel (right).

Fig. 3. Examples of cut and chip wear factors for two wheels with different levels of cut and chip wear. The wheel with red box shows higher cut and chip wear while the wheel with blue box shows lower cut and chip wear. (For interpretation of the references to color in this figure legend, the reader is referred to the Web version of this article.)

Fig. 4. Colloidal plot of tested and reference carbon black grades.

ASTM carbon black grades. These carbon black grades are not tested in this study and are only included in the figure to contextualize the surface area and structure of the tested carbon black grades.

For this work, a naming convention that identifies the structure and surface area of the carbon black is adopted. The carbon black structure measured by compressed oil absorption number, COAN, is listed as the superscript and the carbon black surface area measured by statistical thickness surface area, STSA, is listed as the subscript. For example, N326 carbon black which has a COAN and STSA value of 73 cc.$(100g)^{-1}$ and 76 $m^2\,g^{-1}$ respectively is referred to as CB_{76}^{73}. Table 2 summarizes the values of the CB structure and the CB surface area as well as the adopted

Table 2
CB structure and surface area values, adopted compound naming convention and compound dispersion index.

ASTM grade name	Carbon black/ adopted compound name	Structure (COAN)/cc. $(100\ g)^{-1}$	Surface area (STSA)/m^2. g^{-1}	Compound dispersion index
NA	CB_{117}^{132}	132	117	99.3
NA	CB_{79}^{121}	121	79	98.8
N234	CB_{111}^{108}	108	111	99.4
NA	CB_{145}^{105}	105	145	98.8
N550	CB_{37}^{84}	84	37	98.7
N326	CB_{76}^{73}	73	76	98.0
NA	CB_{161}^{62}	62	161	81.5
NA	CB_{96}^{55}	55	96	90.2

naming convention.

N234, N326 and N550 are ASTM-defined carbon black grades, while the other 5 tested carbon blacks are non-ASTM grades manufactured by Birla Carbon. Most of the tested carbon blacks are used in rubber applications. However, some carbon blacks typically used in ink and coating applications (CB_{96}^{55} and CB_{161}^{62}) were included to broaden the range of colloidal properties, allowing for better understanding and interpolation of the effects of carbon black structure and surface area on cut and chip wear. The compounds were mixed in a three-stage mixing process using a 1.6 L capacity Banbury mixer at Birla Carbon, Marietta, GA, USA. The base formulation for the compounds is shown in Supplementary Table S1 and in previous publications [27,32,33]. The formulation for each compound was identical, with the only difference between the compounds being the type of carbon black grade used. The compounds were mixed in a three-stage mixing process to ensure uniform dispersion of the compounds as detailed in Supplementary Tables S2–S4. Table 2 shows the dispersion index values of the carbon blacks in the final compounds as measured by an interferometric microscope (IFM) technique according to ASTM D2663 (method D) [39]. The compounds show nearly full macro-incorporation of the carbon black in the rubber. The t_{90} of the compounds at 150 °C was measured using a moving die rheometer (MDR) for a period of 30 min.

2.2. Tensile to break characterization

Sheets measuring 110 mm × 110 mm × ~2 mm were vulcanized by compression molding at 150 °C for a time of t_{90} + 5 min. Dumbbells, of approximate gauge length, width and thickness of 25 mm × 6 mm × ~2 mm respectively, were stamped out of the sheets for uniaxial tensile tests to failure following ASTM D412 Standard Test Methods for Vulcanized Rubber and Thermoplastic Elastomers—Tension [40]. Five dumbbell specimens were stretched to failure at an extension rate of 500 mm/min (an approximate strain rate of 0.19/s) using a five-station tensile tester manufactured by Universal Testing Machines with a 1 kN load cell and contact strain gauges. The tensile tests were conducted at atmospheric pressure conditions, room temperature (21 °C ± 1 °C) and 55 % relative humidity.

2.3. Critical tearing energy

The critical tearing energy was measured following ASTM Standard D624-00 Standard Test Method for Tear Strength of Conventional Vulcanized Rubber and Thermoplastic Elastomers [41] using constrained path trouser test specimens developed by Veith [42]. The constrained path trouser test specimens were assembled from green rubber compound and compression molded at 150 °C for a period t_{90} + 5 min and measured approximately 125 mm × 28.5 mm × ~5.33 mm. A longitudinal grove that was about 1.77 mm from the edge of the specimen and about 0.75 mm wide was cut in the specimen to provide a path of least resistance for tear propagation to prevent the tear from growing laterally

and into the leg of the specimen [42]. The legs of the trouser test specimens were reinforced with fabric to minimize elongation in the legs in line with Rivlin and Thomas' assumptions in developing the theory for calculation of critical tearing energy [43].

The critical tearing energy tests were conducted using an Alpha Technologies (model T2000) Tensiometer. A cut of length 60 mm was made down the groove using a razor blade. The legs of the specimens were gripped, and the specimens were torn apart at a grip separation speed of 50 mm/min until the specimen was fully ruptured. The tests were conducted in an environmental chamber at a temperature of 60 °C following a 1-h conditioning time where the specimen was pre-heated in the chamber prior to testing.

As per ASTM D624 [41], the thickness of the specimen was measured by averaging the total thickness of the test piece adjacent to the groove and then subtracting 3.60 mm which represents the combined height of the insert sections that form the groove. The median of the peak forces measured upon tearing the specimen was used for the calculation of critical tearing energy.

2.3.1. Evaluation of critical tearing energy

The evaluation of the critical tearing energy is based on the fracture mechanics theory originally postulated by Griffith [44] and later modified by Rivlin and Thomas [43]. The critical tearing energy, T_c, is an energy criterion below which critical tearing will not occur and is defined by equation (2) where U is the strain energy released upon growth of a crack and da is the new area created upon the growth of the crack.

$$T_c = -\left(\frac{dU}{da}\right)_l \qquad (2)$$

l indicates the growth of a crack at constant length. In practical terms for the trouser tear test specimen, the critical tearing energy, T_c, is obtained as

$$T_c = -\left(\frac{dU}{da}\right)_l = \frac{2\lambda f}{t_0} - wW \qquad (3)$$

Where f is the force applied to the ends of the test specimen, λ is the extension ratio in the legs of the specimen, t_0 is the thickness of the specimen, w is the total width of the specimen and W is the strain energy density in the legs of the specimen. The simplifying assumption adopted by Rivlin and Thomas [43] was that if the total width, w, was chosen to be large enough, the elongation in the legs would be minimal ($\lambda \approx 1$) and W approximates to nearly zero. The critical tearing energy, T_c, in the trouser test specimen therefore simplifies to equation (4). In the constrained path trouser tear specimen, the legs of the specimen are reinforced with fabric - assuring zero leg extension during the test. It is worth pointing out that while ASTM D624 and Veith's calculations omit the factor of 2, it is included in our calculations.

$$T_c = \frac{2f}{t_0} \qquad (4)$$

2.4. Rebound resilience

The rebound resilience was measured using a Zwick Roell 5109 rebound resilience tester. Buttons measuring approximately 25.4 mm in diameter and 12.7 mm in thickness were cured at 150 °C for a time of t_{90} + 10 min and used for the tests. The buttons were initially conditioned in an oven for 1 h at 60 °C. They were removed from the oven and immediately placed at the bottom of the tester against a rigid stainless-steel base. A free-falling hemispherical pendulum hammer with a diameter of ~15 mm was dropped from an angle of 90°. The extent to which the pendulum rebounds is a consequence of the viscoelastic energy dissipation of the material. The average data of 5 repeats for each sample are reported.

2.5. Cut and chip wear testing

The rubber specimens for cut and chip wear testing were compression molded at 150 °C for a time of t_{90} + 13 min.

Table 1 shows proposed test conditions that replicate a specific target application based on calculations in section 5 of the supplementary information. The specific target application was a V-steel Rock Premium Service tire which is designed for rigid dump trucks, a type of earth-mover vehicle. The proposed test values for this specific application condition were the starting point for determining the test conditions on the ICCA.

Trial tests were performed at impact frequencies of 1.5 Hz and 5 Hz, at three applied impact normal forces of 90 N, 110 N and 140 N. A rotational speed of 150 rpm was used instead of the proposed 90 rpm to reduce the testing time for each specimen. Previous testing by Kipscholl and Stoček [45] showed that the rotational speed of the wheel had minimal impact on the cut and chip wear factor. The results of the trial tests are shown in section 7 of supplementary information.

Based on the trial tests, it was determined that impact frequency had minimal effect in changing the ranking of the cut and chip wear of the compounds. An impact frequency of 5 Hz was therefore chosen to reduce the testing time. The trial tests were performed up to 3000 cycles. From the cut and chip wear factor as a function of cycle number (Fig. S3 shown in section 7 of supplementary information), the compounds had not reached a *stabilized* cut and chip wear factor at applied impact normal force of 140 N. The number of cycles was therefore increased to 10,000 cycles to provide enough cycles to obtain a *stabilized* cut and chip wear factor. The time of contact (time that the indenter is in contact with the wheel) was set to 50 ms as per the proposed target application. The sliding speed of the wheel is approximately 0.2 ms⁻¹ based on the time of contact of the indenter and rotational speed of the wheel as calculated in section 6 of supplementary information.

Previous testing by Stoček et al. [46] showed significant differences in the cut and chip damage depending on the severity of the applied impact normal force. Kipscholl and Stoček [45] also showed that the applied impact normal force had the most significant influence on the cut and chip damage. The range of the applied impact normal force was therefore chosen to range from 90 N to 200 N instead of 90 N to 140 N which had been used in the trial tests. The chosen applied impact normal forces were 90 N, 110 N, 125 N, 140 N, 170 N and 200 N. The applied impact normal force was varied while all the other testing conditions were kept constant. Table 3 summarizes the test conditions used on the ICCA. Three repeats were performed for each sample at a given condition. The average data from the three repeats are reported.

2.5.1. Calculation of impact energy

As part of the analysis, the impact energy was calculated to understand the differences in cut and chip wear at low and high applied impact normal forces. The impact energy is an estimate of the energy input into the rubber at each impact stroke and is calculated as

$$\text{Energy input} = \frac{\text{Peak Normal Force} \times \text{Maximum Stroke}}{2} \qquad (5)$$

The peak normal force refers to the peak normal force achieved at each cycle – which is a controlled variable of the ICCA. The maximum

Table 3
Cut and chip wear test parameters.

Parameter	ICCA test parameter values					
	A	B	C	D	E	F
Applied impact normal force/N	90	110	125	140	170	200
Rotational speed/rpm	150					
Impact frequency/Hz	5					
Number of impact cycles	10000					
Time of contact/ms	50					

stroke is the deformation of the indenter into the specimen, and it is measured from the point of contact of the indenter with the specimen to the point it travels into the specimen. A key assumption in this estimation is that frictional energy is minimal compared to normal energy because of the short contact time of 50 ms.

2.6. Cut and chip debris characterization

2.6.1. Particle size analysis of debris

A Malvern Mastersizer 3000 equipped with a Malvern Aero S dry dispersion unit was used to measure the mean particle size of the cut and chip wear debris in dry powder form. The obscuration limit (amount of light blocked or scattered by the particles) was set between 0.01 % and 12.0 %. The particles were fed through a hopper of gap 4 mm into the Malvern Mastersizer with the feed tray vibrating at a rate of 30 % ($\sim$17.4 ms^{-2}) [47]. The particles were circulated in the Malvern Mastersizer at an air pressure of 3 bar. A Fraunhofer approximation was used to calculate the particle size distribution, as it is suitable for large, opaque particles. For each sample, three measurements were performed, and the mean particle size values are reported here.

2.6.2. Optical microscopy of cut and chip debris

A Nikon SMZ1000 optical microscope was used in conjunction with a Lumenera Infinity 1 camera to take images of the cut and chip debris. Teledyne Lumenera Inifinity Analyzer software was used for capturing the images, and the brightness while taking the images was adjusted using a Southern Micro Instruments Fiber Illumination lamp.

3. Results

3.1. Tensile to break characterization

Fig. 5 shows the tensile stress-strain curves of the various carbon black reinforced compounds. The tensile modulus of the compounds strongly correlates with carbon black structure; with high carbon black structure typically leading to higher moduli of the compounds. This is attributed to strain amplification/matrix overstrain effects resulting from rubber occlusion effects of carbon black structure [27,38,48]. The occlusion of rubber increases the effective volume fraction of carbon
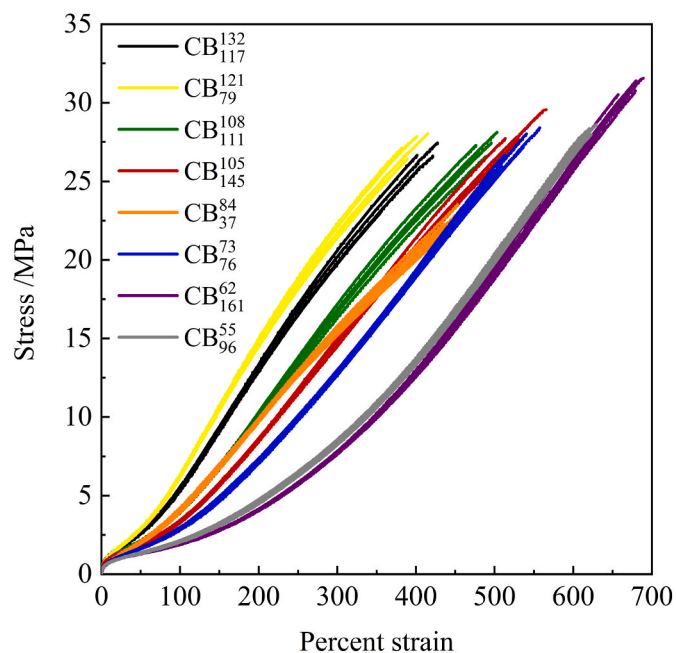
black leading to stiffer compounds which causes a resultant reduction in the elongation at break. The differences in the moduli of the compounds influence the cut and chip wear as is discussed in subsequent sections.

3.2. Critical tearing energy

Fig. 6 shows the critical tearing energy of the various carbon black reinforced compounds.

There are significant differences between the T_c values of the various compounds. Supplementary Table S8 shows the results of multiple regression analysis to determine the effect of carbon black structure and surface area on the measured critical tearing energy. From the results, carbon black structure and carbon black surface area have equal, albeit opposing, influences on the critical tearing energy. While carbon black structure is negatively correlated, carbon black surface area shows a positive correlation with the critical tearing energy.

Increasing carbon black surface area increases the critical tearing energy by increasing the amount of mechanical hysteresis during the tearing process. Increasing carbon black surface area leads to increased particle-particle and particle-polymer interaction which increases irreversible processes such as viscoelasticity and hysteretic breakdown of particulates [31,32]. More energy is thus lost to these processes and higher energy input [49,50] is required for the tearing process causing an increase in the critical tear energy. Carbon black structure increases the stiffness of the compound which is proposed to reduce the effective tip diameter leading to a concomitant reduction in critical tearing energy [7,26,29].

3.3. Rebound resilience

Fig. 7 shows the rebound resilience of the compounds measured at 60 °C. Like the critical tearing energy measurements, multiple regression analysis was performed (as shown in Supplementary Table S9) to determine the effect of carbon black surface area and structure on the rebound resilience which is used as an estimate of the energy dissipation. Based on the statistical analysis, carbon black structure has no effect on the rebound resilience. Carbon black surface area has a significant effect on the rebound resilience, with increasing carbon black surface area increasing the energy dissipation due to increased particle networking.
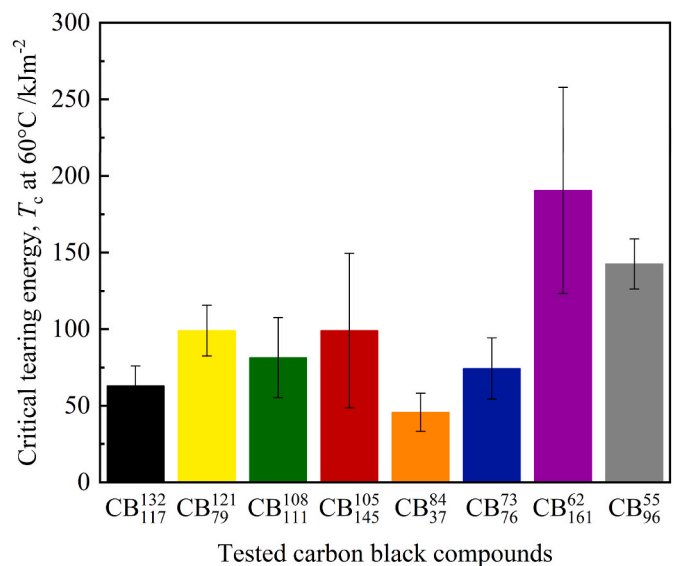

Fig. 5. Tensile stress-strain to failure curves of tested carbon black compounds (reproduced from Kyei-Manu et al. [27]).

Fig. 6. Critical tearing energy, T_c, of tested carbon black compounds. The values and error bars are the average and standard deviation respectively of 5 repeats of each sample.
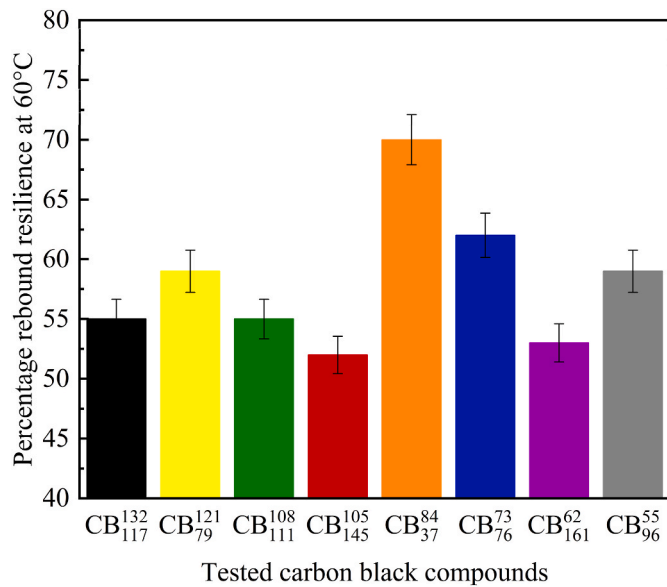
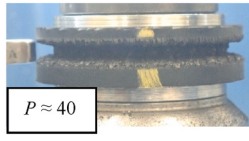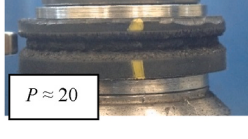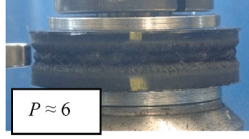**Fig. 7.** Rebound resilience at 60 °C of tested carbon black compounds. The values and error bars are the average and standard deviation respectively of 5 repeats for each sample.

3.4. Cut and chip wear

Fig. 8 shows the cut and chip wear results as measured by the cut and chip wear factor described in section 1.2.1 for each of the six tested applied impact normal forces. The graphs show the average of 3 repeats of each compound at the given applied impact normal force. The error bars show the standard deviation of the 3 repeats. The narrow range of the error bars shows good repeatability of the tests. There are certain key observations from the graphs.

- There are differences in the kinetics of the cut and chip wear between the various compounds and across the studied applied impact normal force range.
- There are significant differences in the steady state cut and chip wear factor (cut and chip wear at 10,000 cycles). For a specific applied impact normal force, the difference in cut and chip wear between the compounds with the lowest and highest cut and chip wear is approximately a factor of 10.
- The ranking of the steady state cut and chip wear factor inverts depending on the severity of the applied impact normal force. For example, at 90 N, the CB_{79}^{121} carbon black compound has the lowest cut and chip wear while the CB_{161}^{62} carbon black compound has the highest cut and chip wear. However, at 200 N, this ranking reverses with the CB_{79}^{121} carbon black compound having the highest cut and chip wear and the CB_{161}^{62} carbon black compound showing the lowest cut and chip wear.

The subsequent sections analyze the cut and chip wear data to explain the observations in Fig. 8 and to better understand the development and progression of the cut and chip phenomenon. This is achieved by looking at some representative images of the tested wheels, correlating the steady state cut and chip wear factor with material properties such as modulus and critical tearing energy, and analyzing characterization of the cut and chip debris.

4. Discussion

4.1. Images of tested cut and chip wheels

Table 4 shows the material properties and the images of two of the tested carbon black compounds (CB_{79}^{121} and CB_{161}^{62}) at the end of the test cycle. These two representative wheels are shown because of the significant differences in their behavior at low and high applied impact
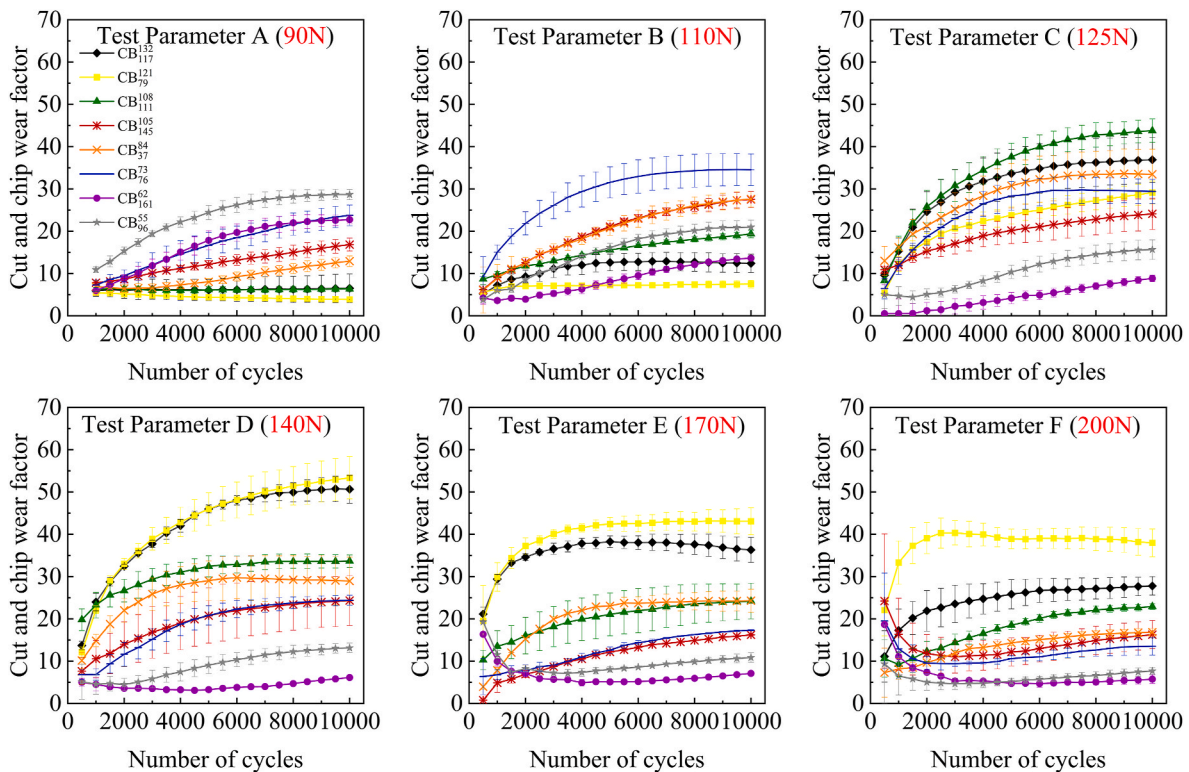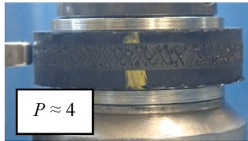
Fig. 8. Cut and chip wear of tested carbon black compounds. The values and error bars are the average and standard deviation respectively of 3 repeats of each sample.

Table 4

Images of CB_{79}^{121} and CB_{161}^{62} wheels after 10,000 cycles at 90 N and 200 N.

Carbon black type	Compound properties	10,000 cycles at 90 N	10,000 cycles at 200 N

CB_{79}^{121}
   Structure: High
   Surface Area: Low
	M100 = 6.35 MPa
	T_c = 99.04 kJm^{-2}
	
	[a]RR = 59 %
		$P \approx 4$	$P \approx 40$

CB_{161}^{62}
   Structure: Low
   Surface Area: High
	M100 = 1.90 MPa
	T_c = 190.54 kJm^{-2}
	
	[a]RR = 53 %
		$P \approx 20$	$P \approx 6$

[a] RR refers to the rebound resilience. A higher percentage means lower energy dissipation.

normal forces. The images show significant differences in their cut and chip wear with applied impact normal force.

The CB_{79}^{121} and CB_{161}^{62} carbon black compounds show significant differences in their modulus (M100 – stress value at 100 % extension) and critical tearing energy properties. The CB_{79}^{121} compound which is reinforced with a carbon black that has a high structure and low surface area has a higher modulus and lower critical tearing energy while the CB_{161}^{62} compound reinforced with a low structure and high surface area carbon black has a lower modulus and higher critical tearing energy. The CB_{79}^{121} carbon black compound has higher percentage rebound resilience (lower energy dissipation) compared to the CB_{161}^{62} carbon black compound.

The differences in material properties influence the extent of cut and chip wear of the compounds as shown in the images of the wheels after testing at 90 N and 200 N. The CB_{79}^{121} carbon black compound has the lowest cut and chip wear at 90 N which is reflected in the comparatively undamaged surface of the wheel after 10,000 cycles. The surface of the wheel shows cracking but minimal material loss.

However, at 200 N, the wheel of the CB_{79}^{121} carbon black compound shows larger variation in surface roughness with a substantial volume of rubber having been removed. The wheel of the CB_{161}^{62} carbon black compound shows less variation in the cut and chip wear at 90 N and 200 N. The surface of the wheels exhibits some material loss at both 90 N and 200 N but the variation in surface roughness is relatively similar.

It is important to discuss crack formation on the CB_{79}^{121} rubber wheel tested at low applied impact normal forces (defined in this paper as 90 N and 110 N). Table 4 shows the wheel after testing for 10,000 cycles at applied impact normal force of 90 N. Additionally, Table S10 in supplementary information shows the evolution of the cracks on the surface of the CB_{79}^{121} rubber wheel tested at applied impact normal force of 110 N at various cycles (before testing, 100 cycles, 500 cycles, 1000 cycles, 2000 cycles, 5000 cycles and 10000 cycles). The evolution of the development of the cracks at low applied impact normal force (90 N and 110 N) are similar. Cracks begin to develop on the wheel's surface at about 500 cycles, forming at distinct angles. As they grow in length and number, the cracks intersect, leading to the removal of small chips of rubber from the wheel's surface [46,51].

The distinct angles of the cracks on the rubber wheel contrast with previously published findings on SBR compounds [46,51]. Stoček et al. [46,51] showed that initiated cracks in SBR rubber wheels were vertically oriented across the impact path.

4.2. Steady state cut and chip wear

To analyze the cut and chip deformation and to understand the transition in behavior and material ranking with increasing applied impact normal force, the "steady state" cut and chip wear is examined.

The steady state cut and chip wear is the cut and chip wear factor value at 10,000 cycles. For reference, the cut and chip wear measured by the change in mass of the wheels after 10,000 cycles is shown in Supplementary Fig. S5, along with a brief discussion comparing it to the steady state cut and chip wear factor. Fig. 9 shows the steady state cut and chip wear factor of the compounds as a function of applied impact normal force.

There are three key observations from Fig. 9.

- Generally, there are peaks in the cut and chip wear with increasing applied impact normal force.
- There is an inversion of the material performance ranking going from low to high applied impact normal force.
- There is a complex relationship between applied impact normal force and compound properties with the trends becoming clearer when the steady state cut and chip wear of the compounds are grouped by the static tensile modulus as shown in Fig. 10.

The peak in the cut and chip wear for the high modulus compounds occurs at a higher applied impact normal force of 140 N while the peak
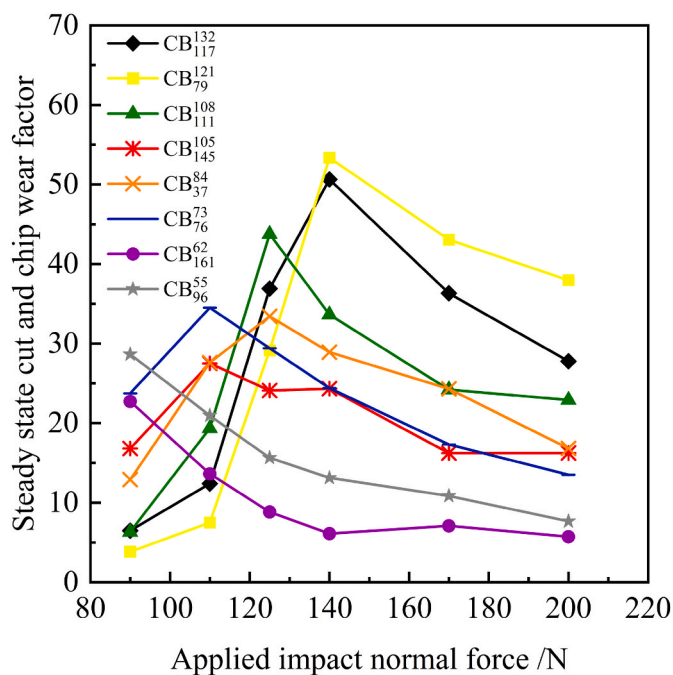

Fig. 9. Steady state cut and chip wear at different applied impact normal forces.
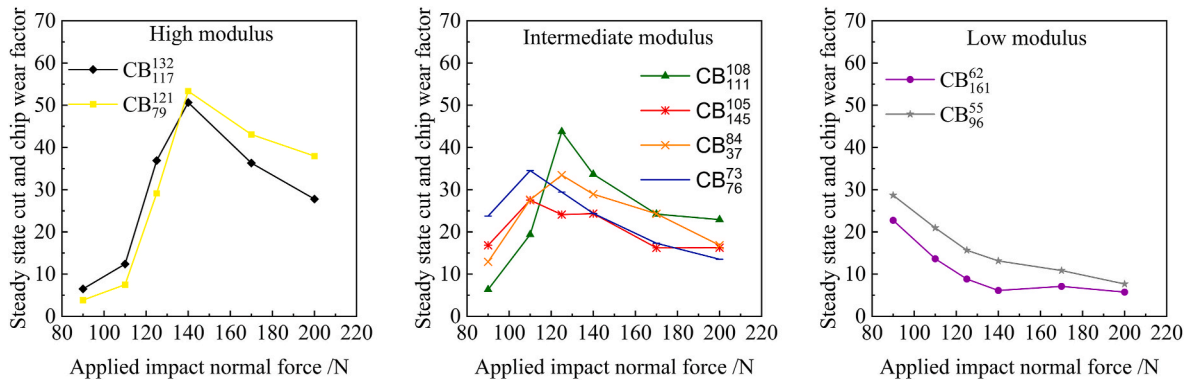
Fig. 10. Steady state cut and chip wear at different applied impact normal forces separated by modulus.

in the intermediate modulus compounds occurs at slightly lower applied impact normal forces of 110 N or 125 N. There is no transition observed for the low modulus compounds with the cut and chip wear decreasing with increasing applied impact normal force, with any transition seemingly occurring below the minimum force level used in these experiments.

These observations can be rationalized by considering the role of strain induced crystallization in cut and chip wear. Stoček and al [46]. performed cut and chip wear measurements on three different compounds: a strain crystallizing compound (NR), a non-crystallizing compound (SBR) and a 50-50 blend of the two compounds. The graph of the steady state cut and chip wear of the 3 different compounds with increasing applied impact normal force is reproduced in Supplementary Fig. S7. From the graph, the strain crystallizing compound and the 50-50 blend showed a peak in the cut and chip wear with increasing applied impact normal force similar to what is observed in Figs. 9 and 10. The non-crystallizing compound showed a monotonic increase in cut and chip wear, increasing with increasing applied impact normal force. One plausible explanation for the peak in cut and chip wear is the onset of crystallization – a strain activated toughening mechanism which helps to inhibit the cut and chip wear once it occurs.

The cut and chip instrument uses a force-controlled indenter, applying a set force to the rubber specimen with each impact, making it a force/stress-controlled experiment. Under stress-controlled deformation, softer/low modulus compounds tend to deform to higher strains than stiffer/high modulus compounds [52–54]. Consequently, at a given applied impact normal force, strain levels in the low modulus compounds are generally higher compared to the high modulus compounds. It is argued that the onset of crystallization occurs at a lower applied impact normal force for the low modulus compounds compared to the high modulus compounds due to further deformation and the consequent higher strain levels [55]. This may explain why the peak of the intermediate compounds occurs at lower applied impact normal forces compared to the peak of the high modulus compounds. The low modulus compounds show a decreasing cut and chip wear with increasing applied impact normal force possibly because the onset of crystallization occurs prior to the lowest tested applied impact normal force of 90 N.

4.3. Material and test property correlations to understand cut and chip

4.3.1. Critical tearing energy and steady state cut and chip wear

To understand the mechanisms that dominate cut and chip wear, the steady state cut and chip wear factors are plotted as a function of the critical tearing energy values discussed in section 3.2. Fig. 11 shows the plot on a log-log scale. A line of best fit is drawn with the R^2 values indicated to show the correlation between the steady state cut and chip
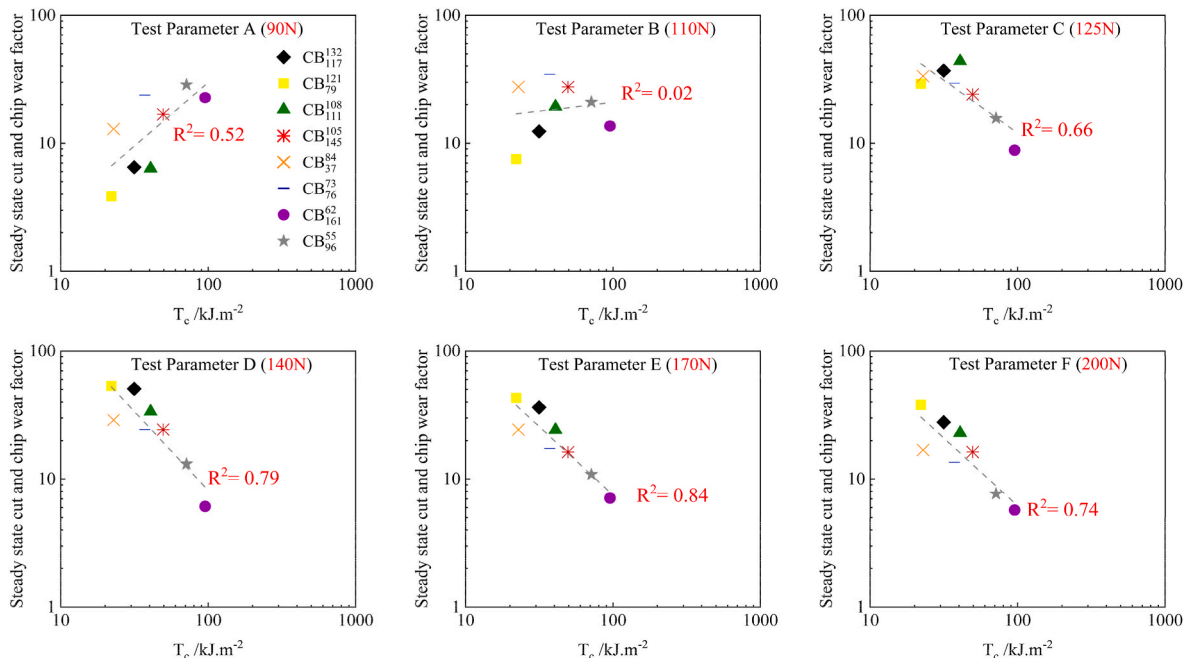

Fig. 11. Steady state cut and chip wear as a function of critical tearing energy on a log-log scale.

wear and the critical tearing energy.

At low applied impact normal forces (≤ 125N), the steady state cut and chip wear does not correlate with the critical tearing energy. Although there is a poor correlation between the steady state cut and chip wear at 90 N and the critical tearing energy, it is noteworthy that the relationship is positive; higher critical tearing energy leads to higher cut and chip wear. The positive relationship between the cut and chip wear appears to change at an applied impact normal force of about 125 N. At higher applied impact normal forces (≥ 140N), the steady state cut and chip wear correlates with the critical tearing energy with R^2 values ≥ 0.74. Under these impact conditions, the higher the critical tearing energy of the compound, the lower the steady state cut and chip wear that is observed.

This suggests that possibly two different mechanisms dominate cut and chip performance depending on the applied impact normal force. At high applied impact normal forces, the cut and chip deformation is dominated by a critical tearing mechanism. This correlation between cut and chip wear and the critical tearing energy has been reported by previous researchers. Veith [42] reported good correlation between cut and chip performance rating of off-road tires as a function of their critical tear energy measured at 60 °C. Recently, Deuri et al. [15] reported a similar indirect relationship of critical tearing energy and cut and chip wear (as measured by mass loss of the tested compounds) for fiber reinforced compounds. For the first time however, in this paper it is shown that the dependence of cut and chip wear to critical tearing energy is also dependent on the applied impact normal force. The correlation between the steady state cut and chip wear and the critical tearing energy is also reflective of the effects of strain induced crystallization, where typically crystallization at the crack tip is an effective reinforcing mechanism to minimize the tearing action.

4.3.2. Impact energy and steady state cut and chip wear

The cut and chip wear factor is plotted against the calculated impact energy to assess how the input energy during the cut and chip testing affects the recorded wear. Fig. 12 illustrates the cut and chip wear factor

recorded after 1000 cycles in increments of 500 cycles as a function of the impact energy at the corresponding cycle number.

At low applied impact normal forces, the cut and chip wear is directly proportional to impact energy, with increasing impact energy leading to increasing cut and chip wear irrespective of the type of carbon black. All compounds, at all stages of the cut and chip experiment collapse onto an apparent master-line. This is similar to a force-controlled fatigue life experiment where increasing energy input increases the crack growth rate and reduces fatigue life. Under these conditions, stiff compounds perform best as they minimize deflection under force control and therefore minimize impact energies. As the applied impact normal force increases, the master-line correlation with the impact energy begins to break down with increasing differentiation between the cut and chip wear based on the type of carbon black. With increasing applied impact normal force, the high structure carbon black compounds such as CB_{117}^{132} and CB_{79}^{121} exhibit higher cut and chip wear at a given applied impact energy.

Based on the evaluation of the cut and chip wear with critical tearing energy and impact energy, two different mechanisms appear to dominate cut and chip wear depending on the severity of applied impact normal force. At low applied impact forces (≤ 125 N), cut and chip wear is dominated mostly by a force controlled, fatigue crack growth mechanism while at high applied impact forces (≥ 125 N), cut and chip wear is dominated by a critical tearing mechanism.

4.4. Effect of carbon black properties on steady state cut and chip

Multiple regression analysis of the cut and chip wear with regards to carbon black structure and surface area was performed to determine the influence of carbon black morphological properties on the steady state cut and chip wear. Multiple linear regression analysis was performed as per equation (6) where Y is the dependent variable (in this case the cut and chip wear), C is an intercept constant, β_{St} (COAN) is the coefficient of structure of carbon black, β_{SA} (STSA) is the coefficient of the surface area of carbon black and ε is the error term.
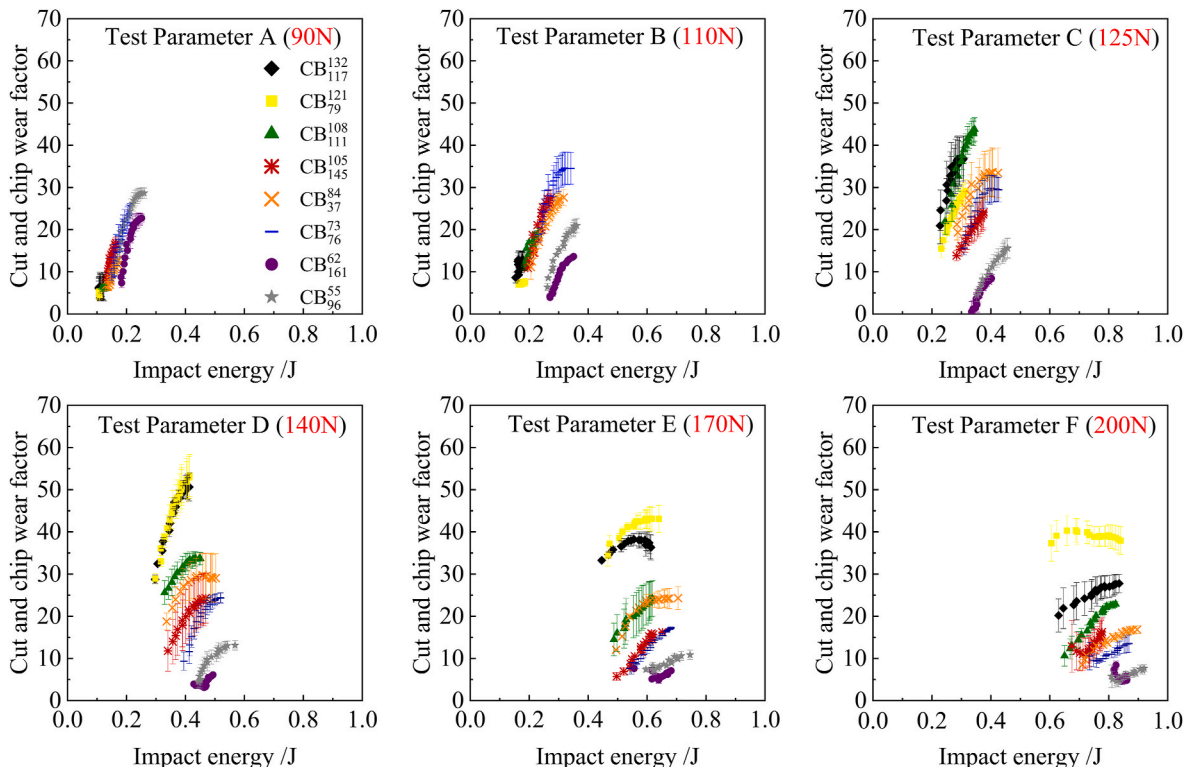

Fig. 12. Cut and chip wear as a function of impact energy.

$$Y = \beta_{St}(COAN) + \beta_{SA}(STSA) + C + \epsilon \qquad (6)$$

Fig. 13 shows the normalized regression coefficients as a function of the applied impact normal force. The coefficient values that do not show a statistical correlation are shown as open symbols. Positive normalized coefficient values suggest increasing that property increases the cut and chip wear (decreases cut and chip resistance) while negative normalized coefficient values suggest increasing that property decreases cut and chip wear. The closer the value is to 0, the lower the influence, while the closer the value is to 1 or -1, the higher the influence.

From the regression results, the effect of carbon black structure and surface area on cut and chip wear varies depending on the level of applied impact normal force, similar to earlier discussions in this paper. Carbon black structure has the stronger albeit opposing effect (depending on the level of applied impact normal force) on cut and chip wear. At low applied impact normal force of 90 N, increasing carbon black structure decreases cut and chip wear. At 110 N, there is no statistical influence of carbon black structure on cut and chip wear, probably because this applied impact normal force is in the vicinity of the transition in cut and chip mechanism. Above 110 N applied impact normal force, increasing carbon black structure increases cut and chip wear. At low applied impact normal force, high carbon black structure which produces high modulus compounds which deflect less under force thus decreasing cut and chip wear is preferred. At high applied impact normal forces, low carbon black structure which produce low modulus compounds that can strain crystallize more and thus decrease cut and chip wear is preferred. Another likely reason low structure carbon black compounds are preferred over high structure carbon black compounds at high impact normal forces could be due to lamellar flaking. This is discussed in more detail in section 4.5 as part of the debris characterization results.

Based on the regression analysis, carbon black surface area influences the cut and chip wear at high applied impact normal forces. Increasing carbon black surface area, decreases cut and chip wear. High surface area carbon black compounds typically lead to high hysteresis (energy dissipation) as evidenced by the rebound resilience results and thus more energy is dissipated when deforming the rubber material.

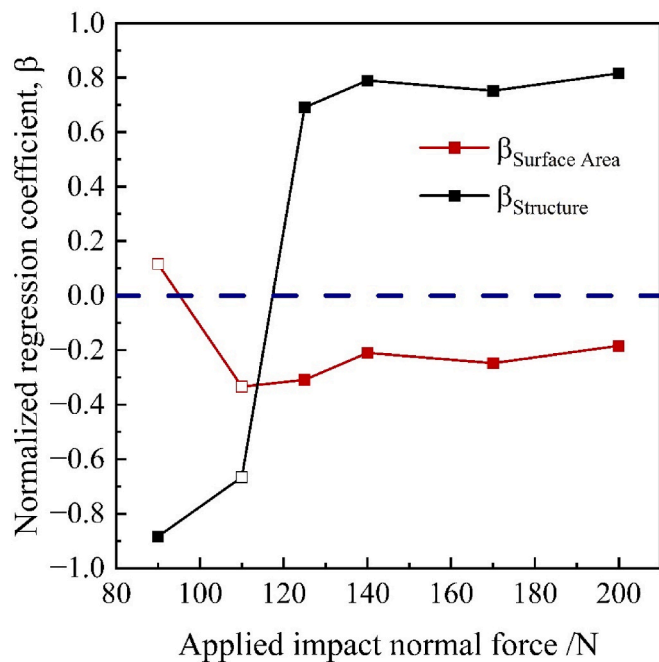Based on the regression results, design guidelines to minimize cut and chip wear can be provided as shown in Table 5.

At low applied impact normal force, compounds reinforced with high structure carbon blacks which minimize deflection under load reduce cut and chip wear. At high applied impact normal forces, compounds reinforced with low structure and high surface area carbon blacks which strain crystallize more and increase energy dissipation reduce cut and chip wear. The preferred carbon black properties to minimize cut and chip wear at high severity (i.e., higher surface area, lower structure) are in good agreement with carbon blacks such as N220 or N115 historically used for off road, high severity applications. They are, however, in contradiction to those typically utilized for good road wear performance. Previous researchers [4,12,51] have reported similar observations where tested compounds that provided good cut and chip resistance were poor for fatigue and abrasive wear. This work identifies the specific applied impact normal force range in which these types of compounds are preferred, enabling the selection of appropriate compound properties for cut and chip wear based on the anticipated force levels encountered in the field. It is evident that to select the appropriate carbon black and compound properties to minimize cut and chip wear, it is critical to understand the severity of the application.

4.5. Debris characterization

4.5.1. Particle size analysis of debris

Table S11 in supplementary information shows the values of the mean particle size of the debris at four different applied impact normal forces where debris were collected. Cut and chip debris was not collected at 110 N and 170 N. At 90 N, three of the compounds did not have enough debris to be analyzed on the Mastersizer.

The steady state cut and chip wear factor of the compounds at the 4 applied impact normal forces are plotted as a function of the mean particle size of the debris in Fig. 14. At high applied impact normal force ($\geq$125 N), the steady state cut and chip wear correlates well with cut and chip wear debris. Higher steady state cut and chip wear leads to larger cut and chip debris particle size.

The correlation of the steady state cut and chip wear with the mean particle size of the debris at higher applied impact normal forces provides further evidence that at high applied impact normal force, the cut and chip wear is dominated by tearing away or chunking of the material.

4.5.2. Optical microscopy images of debris

Fig. 15 shows images of the cut and chip debris of two of the carbon black reinforced compounds (CB_{79}^{121}, a high structure carbon black compound and CB_{161}^{62}, a low structure carbon black compound) from tests performed at 200 N. Table S12 in supplementary information shows images of the debris for the other carbon black compounds collected at 140 N and 200 N.

The debris shows differences in size and morphology dependent on the modulus of the compounds, which based on previous discussions is influenced by the structure of the carbon black. The debris of high modulus (structure) compounds such as CB_{79}^{121} are large chunks while the debris of low modulus (structure) compounds such as CB_{161}^{62} are small and powdery.

This observation provides some insight into why, at higher applied impact normal forces, high-structure carbon black compounds tend to exhibit worse cut and chip wear. Fujimoto et al. [56] studied the anisotropy of dynamic and fracture properties on fracture mechanisms.

Fig. 13. Normalized regression coefficients showing effects of carbon black structure and surface area on cut and chip wear.

Table 5
Carbon black selection recommendations to minimize cut and chip wear.

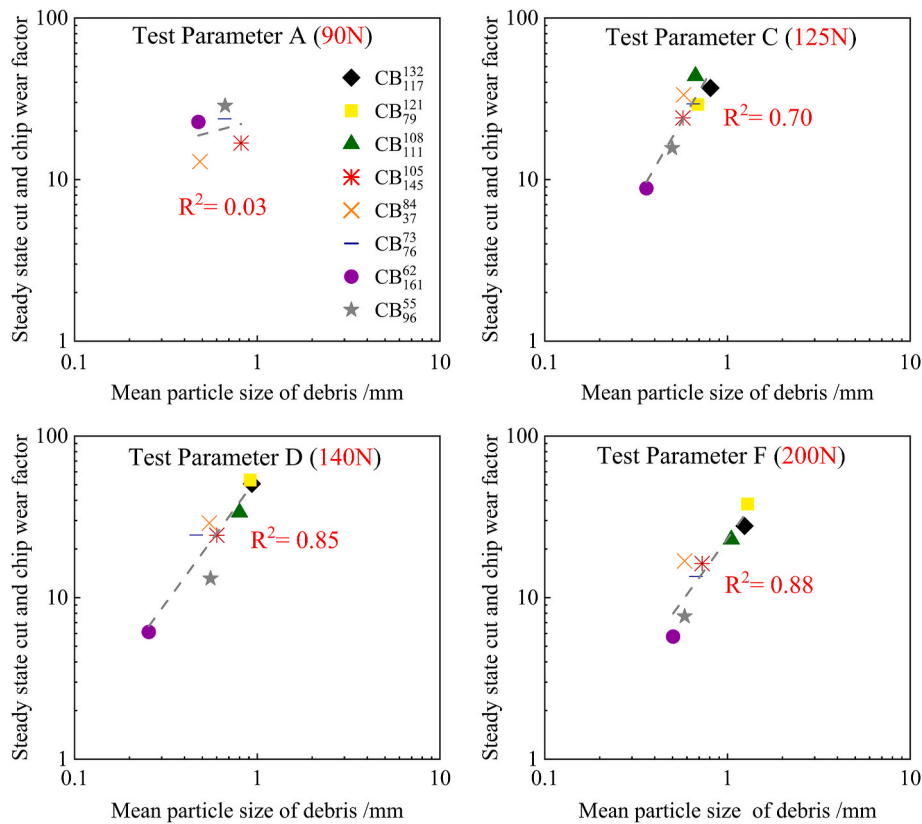| Level of applied impact normal force	Proposed carbon black properties	
	CB structure	CB surface area
Low ($\leq$125N)	Increase	–
High ($\geq$125N)	Decrease	Increase

Fig. 14. Steady state cut and chip wear as a function of the mean particle size of cut and chip debris on a log-log scale.
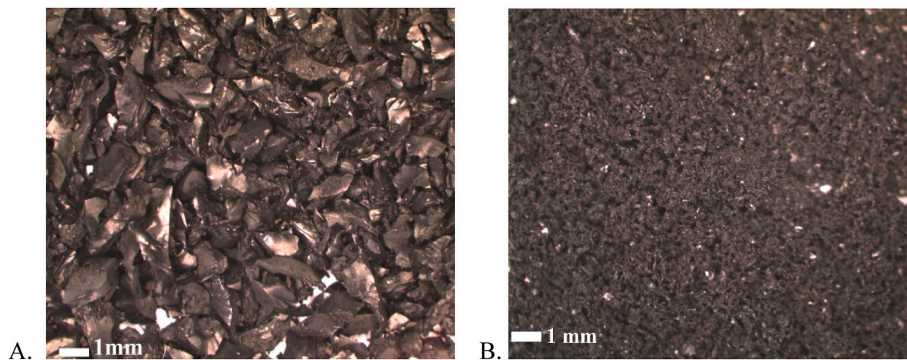

Fig. 15. Optical microscopy images of cut and chip debris of A. CB_{79}^{121} carbon black compound and B. CB_{161}^{62} carbon black compound tested at 200 N.

They found that when an anisotropic layer structure is formed to some critical degree, cracks generate on the sample surface perpendicular to the principal stresses (that is perpendicular to the layer structure). The cracks grow parallel to the layer structure as fatigue progresses and consequently lamellar flaking appears on the surface and yields striped patterns of fatigue fracture. As the anisotropic properties of the structure and the degree of fatigue got more pronounced, the lamellar fractures were more easily generated by low stresses. Supplementary Fig. S8 reproduces an image that describes the fatigue fractures for particle-reinforced rubber composites due to three-dimensional stresses as described above.

High structure carbon blacks, because of their morphology (highly branched structures) can rotate and align with the direction of the stress forming a lamellar structure. Strain induced crystallization further enhances this anisotropy in natural rubber. At high applied impact normal forces, the cracks that develop during cut and chip wear in high structure carbon black compounds could result in lamellar flaking fractures.

This could explain why at high applied impact normal forces, high structure carbon black compounds exhibit higher cut and chip wear following the onset of strain induced crystallization. This failure description during cut and chip wear at high applied impact normal force may also explain why debris size and critical tearing energy correlate with cut and chip wear at high applied impact normal force.

As was previously shown, at high applied impact normal force, the surface area of carbon black which predominantly determines the level of energy dissipation starts influencing the observed cut and chip wear. The powdery form of the debris of the low modulus compounds versus the chunkier forms of the debris of the high modulus compounds also gives some insight into the influence of surface area minimizing cut and chip wear at high applied impact normal forces. The powdery form of the debris of the low modulus compounds hints at more fracture surface area for these compounds. This means there is more energy dissipation and less energy to deform the compound compared to the high modulus compounds.

5. Conclusions

The effect of carbon black colloidal properties on cut and chip wear of natural rubber compounds were studied using an Instrumented Cut and Chip Analyzer (ICCA). The cut and chip wear was characterized using a cut and chip wear factor which indirectly measured the variation in surface roughness of the specimen.

The observed levels of cut and chip wear are dependent on the severity of applied impact normal force. The various natural rubber compounds showed an increase and then a decrease of cut and chip wear with increasing applied impact normal force. Also, the ranking of the compounds with regards to which are most resistant to cut and chip wear is reversed with increasing applied impact normal force. At low applied impact normal forces (≤ 125 N), high structure carbon black compounds are preferred while at high applied impact normal forces (≥ 125N), low structure carbon black compounds are preferred.

These observations can be rationalized by considering strain induced crystallization effects. At low applied impact normal forces, before the onset of strain induced crystallization, high structure carbon black compounds are preferred because they result in stiffer compounds that can minimize deflection in a force-controlled experiment. However, at high applied impact normal forces, after the onset of strain induced crystallization, low structure carbon black compounds are preferred, as they deform more and may form a greater level of crystallites, which minimize cut and chip wear.

At low applied impact normal forces, cut and chip wear increases linearly with the impact (input) energy, irrespective of carbon black type. However, at high applied impact normal forces, this correlation breaks down and cut and chip wear correlates with critical tearing energy, with increasing critical tearing energy leading to lower cut and chip wear. Based on these observations, it is proposed that there is a transition in the cut and chip wear from a force-controlled fatigue crack growth mechanism at low applied impact normal forces to a tearing dominated mechanism at high applied impact normal forces.

CRediT authorship contribution statement

William Amoako Kyei-Manu: Writing – original draft, Visualization, Validation, Supervision, Methodology, Investigation, Formal analysis, Data curation. **Lewis B. Tunnicliffe:** Writing – review & editing, Validation, Supervision, Resources, Project administration, Methodology, Investigation, Formal analysis, Data curation, Conceptualization. **Charles R. Herd:** Writing – review & editing, Validation, Supervision, Resources, Project administration, Funding acquisition, Conceptualization. **Keizo Akutagawa:** Writing – review & editing, Validation, Supervision, Methodology, Formal analysis. **Radek Stoček:** Writing – review & editing, Validation, Supervision, Project administration, Methodology, Investigation, Formal analysis, Conceptualization. **James J.C. Busfield:** Writing – review & editing, Validation, Supervision, Resources, Project administration, Funding acquisition, Conceptualization.

Declaration of competing interest

The authors declare the following financial interests/personal relationships which may be considered as potential competing interests: William Amoako Kyei-Manu reports financial support and equipment, drugs, or supplies were provided by Birla Carbon Inc., Marietta GA. William Amoako Kyei-Manu reports a relationship with Birla Carbon Inc., Marietta GA that includes: funding grants. If there are other authors, they declare that they have no known competing financial interests or personal relationships that could have appeared to influence the work reported in this paper.

Appendix A. Supplementary data

Supplementary data to this article can be found online at https://doi.org/10.1016/j.wear.2024.205673.

Data availability

Data will be made available on request.

References

[1] G. Heinrich, M. Klüppel, Basic mechanisms and predictive testing of tire-road abrasion, in: Degradation of Elastomers in Practice, Experiments and Modeling, vol. 289, Advances in Polymer Science, Springer, Cham, 2022.

[2] Michelin North America Inc, Michelin Truck Tire Service Manual, 2017.

[3] J. Beatty, B. Miksch, A laboratory cutting and chipping tester for evaluating off-the-road and heavy-duty tire treads, in: Rubber Division, American Chemical Society, 1982. Philadelphia.

[4] S. Ahmad, Z.S. Lee, S.E. Katrenick, United States Patent 703 (4) (1987), 079.

[5] E. Euchler, H. Michael, M. Gehde, O. Kratina, R. Stoček, Wear of technical rubber materials under cyclic impact loading conditions, Kautsch. Gummi Kunstst. 69 (2016) 22–26.

[6] Bridgestone, Databook: off the road tires. Off the Road Tire Department, Bridgestone Corporation, Tokyo, 2022.

[7] M.-J. Wang, M. Morris, Rubber Reinforcement with Particulate Fillers, Hanser, 2021.

[8] R. Stoček, W.V. Mars, C.G. Robertson, Characterizing Rubber's Resistance against Chip and Cut Behavior, Rubber World, 2018, pp. 38–40.

[9] R. Stoček, G. Heinrich, A. Schulze, M. Wunde, M. Klüppel, C. Vatterott, J. Tschimmel, J. Lacayo-Pineda, R. Kipscholl, Chip & cut wear of truck tire treads: comparison between laboratory and real tire testing, KGK Rubberpoint (June 2020) 51–55.

[10] R. Kipscholl, R. Stoček, Degradation of tires during intended usage, in: Degradation of Elastomers in Practice, Experiments and Modeling vol. 289, Advances in Polymer Science, Springer Cham, 2022.

[11] C. Nah, B. Jo, S. Kaang, Cut and Chip resistance of NR-BR blend compounds, J. Appl. Polym. Sci. (1998) 864–872.

[12] E. Kasi, F.X. Josephraj, A.K. Murugesan, B. Pandian, Effect of crosslink density on cut and chip resistance of 100% SBR based tire tread compound, Mater. Plast. 58 (1) (2021) 34–46.

[13] M. Pöschl, R. Stoček, P. Zádrapa, The effect of apparent cross-link density on cut and chip wear in natural rubber, in: Degradation of Elastomers in Practice, Experiments and Modelling, Springer, Cham, 2022, pp. 273–291.

[14] M. Pöschl, R. Stoček, P. Zádrapa, M. Stěnička, G. Heinrich, How is cut and chip wear influenced by the variation of the cross-link density within the conventional vulcanization system of natural rubber? Express Polym. Lett. 18 (12) (2024) 1178–1190.

[15] A.S. Deuri, K. Vineet, K. Morankar, D. Vaidya, A. Sourabh, A.K. Bhowmick, Cut and Chip Properties of Tire Rubber Compounds, KGK Rubber point, January/February 2021.

[16] M.L. Engelhardt, K.D. Kim, K. Ho Son, K. Baranwal, R. Samples, Evaluation of filler reinforcements to improve cutting and chipping resistance of tire treads, in: ITEC September 1996, 1996.

[17] R. Stoček, P. Ghosh, A. Machu, J. Chanda, R. Mukhopadhyay, Fatigue crack growth vs. Chip and cut wear of NR and NR/SBR blend-based rubber compounds, in: Fatigue Crack Growth in Rubber Materials: Experiments and Modelling, vol. 286, Springer International Publishing AG, 2021, pp. 225–244.

[18] N. Ryzí, R. Stoček, J. Maloch, M. Stěnička, How does heat generation affect the cut and chip wear of rubber? Polym. Bull. (2024).

[19] K. Swogger, A. Krupp, Material to Give Tire Compounds Lower Density, Lower Hysteresis and Improved Wear, Rubber & Plastics news, 5 April 2021, pp. 16–17.

[20] R. Stoček, R. Kipscholl, E. Euchler, G. Heinrich, Study of the relationship between fatigue crack growth and dynamic chip & cut behavior of reinforced rubber materials, KGK Kautschuk Gummi Kunststoffe 67 (April 2014) 26–29.

[21] C.G. Robertson, J.D. Suter, M.A. Bauman, R. Stoček, W.V. Mars, Finite element modeling and critical plane analysis of a cut-and-chip experiment for rubber, Tire Sci. Technol. 49 (2) (2021) 128–145.

[22] J.-H. Ma, S.-H. Zhao, L.-Q. Zhang, Y.-P. Wu, Comparison of structure and properties of two styrene-butadiene rubbers filled with carbon black, carbon-silica dual phase filler, and silica, Rubber Chem. Technol. 86 (4) (2013) 664–678.

[23] R. Datta, Improving cut/chip/chunk resistance in truck tyres by the use of para-amid chopped fibres, Int. Polym. Sci. Technol. (2005) 10–18.

[24] J.-H. Ma, Y.-X. Wang, L.-Q. Zhang, Y.-P. Wu, Improvement of cutting and chipping resistance of carbon black-filled styrene butadiene rubber by addition of nanodispersed clay, J. Appl. Polym. Sci. 125 (2012) 3484–3489.

[25] N.S. Chundawat, B.S. Parmar, A.S. Deuri, D. Vaidya, S. Jadoun, P. Zarrintaj, M. Barani, N.P.S. Chauhan, Rice husk silica as a sustainable filler in the tire industry, Arabain Journal of Chemistry 15 (9) (2022).

[26] J.-B. Donnet, R.C. Bansal, M.-J. Wang, Carbon Black: Science and Technology, Marcel Dekker, New York, 1993.

[27] W. Kyei-Manu, C. Herd, M. Chowdhury, J. Busfield, L. Tunnicliffe, The influence of colloidal properties of carbon black on static and dynamic mechanical properties of natural rubber, Polymers 14 (1194) (2022).

[28] K.J. Rutherford, K. Akutagawa, J.L. Ramier, L.B. Tunnicliffe, J.J. Busfield, The influence of carbon black colloidal properties on the parameters of the kraus model, Polymers 15 (7) (2023) 1675.

[29] L.B. Tunnicliffe, Fatigue crack growth of carbon black-reinforced natural rubber, Rubber Chem. Technol. 94 (3) (2021) 494–514.

[30] W. Kyei-Manu, P. Hurrell, K. Akutagawa, J. Busfield, C. Herd, L. Tunnicliffe, Effect of carbon black properties on the abrasion resistance of rubber compounds at low sliding speed, in: Constitutive Models for Rubber XII Proceedings of the 12th European Conference on Constitutive Models for Rubber (ECCMR 2022), CRC Press, Milano, 2022.

[31] W.A. Kyei-Manu, L.B. Tunnicliffe, J. Plagge, C.R. Herd, K. Akutagawa, N.M. Pugno, J.J. Busfield, Thermomechanical characterization of carbon black reinforced rubbers during rapid adiabatic straining, Frontiers in Materials 421 (2021).

[32] W. Kyei-Manu, L. Tunnicliffe, C. Herd, K. Akutagawa, O. Kratina, R. Stoček, J. Busfield, Effect of carbon black on heat build-up and energy dissipation in rubber materials, in: Advances in Polymer Science, Springer, Berlin, Heidelberg, 2024.

[33] J.-B. Le Cam, W.A. Kyei-Manu, A. Tayeb, P.-A. Albouy, J.J. Busfield, Strain-induced crystallisation of reinforced elastomers using surface calorimetry, Polym. Test. 131 (2024).

[34] ASTM International, *ASTM Standard D3849 Standard Test Method for Carbon Black-Morphological Characterization of Carbon Black Using Electron Microscopy,* West Conschohocken, Pennsylvania: Annu, Book ASTM Stand., 2016.

[35] ASTM International, *ASTM Standard D6556 Standard Test Method for Carbon Black-Total And External Surface Area by Nitrogen Adsorption,* West Conshohocken, Pennsylvania: Annu, 09.01, Book ASTM Stand, 2019.

[36] ASTM International, *ASTM Standard D2414 Standard test method for carbon black oil absorption number (OAN),* West Conshohocken, Pennsylvania: annu, Book ASTM Stand. 09.01 (2019).

[37] ASTM International, ASTM standard D3493 standard test method for carbon black - oil absorption number of compressed sample (COAN), west conshohocken, Pennsylvania: annu, Book ASTM Stand 09.01 (2019).

[38] A.I. Medalia, Effect of carbon black on dynamic properties of rubber vulcanizates, Rubber Chem. Technol. 51 (3) (1978) 437–523.

[39] ASTM International, ASTM Standard D2663 Standard Test Methods for Carbon Black- Dispersion in Rubber, Annu. Book ASTM Stand, West Conshohocken, 2019, 09.01.

[40] ASTM International, ASTM Standard D412 Standard Test Methods for Vulcanized Rubber and Thermoplastic Elastomers-Tension, Annual Book of ASTM Standards, West Conshohocken, 2002, 03.01.

[41] ASTM International, *ASTM D624-00*(2020) *Standard Test Method For Tear Strength Of Conventional Vulcanized Rubber And Thermoplastic Elastomers,* West Conschohocken, Pennsylvania: Annu, Book ASTM Standard, 2020.

[42] A.G. Veith, A new tear test for rubber, Rubber Chem. Technol. 38 (4) (1965) 700–718.

[43] R. Rivlin, A. Thomas, Rupture of rubber. I. Characteristic energy for tearing, J. Polym. Sci. 10 (3) (1953) 291–318.

[44] A.A. Griffith, VI. The phenomena of rupture and flow in solids, Philos. Trans. R. Soc. Lond. - Ser. A Contain. Pap. a Math. or Phys. Character 221 (1921) 163–198.

[45] R. Kipscholl, R. Stoček, Quantification of chip and cut behaviour of basic rubber (NR, SBR), RFP Rubber Fibers Plastics 2 (2019) 88–91.

[46] R. Stoček, G. Heinrich, R. Kipscholl, O. Kratina, Cut & chip wear of rubbers in a range from low up to high severity conditions, Applied Surface Science Advances 6 (2021) 100152.

[47] Malvern Panalytical, *Malvern Panalytical Mastersizer 3000+ Brochure*, Worcestershire, 2004.

[48] M.-J. Wang, S. Wolff, E.-H. Tan, Filler-elastomer interactions. Part VIII. The role of the distance between filler aggregates in the dynamic properties of filled vulcanizates, Rubber Chem. Technol. (1993) 178–195.

[49] K. Grosch, J. Harwood, A. Payne, Breaking energy of rubbers, Rubber Chem. Technol. 40 (3) (1967) 815–816.

[50] J.-B. Le Cam, Fast evaluation and comparison of the energy performances of elastomers from relative energy stored identification under mechanical loadings, Polymers 14 (3) (2022) 412.

[51] R. Stoček, W.V. Mars, R. Kipscholl, C.G. Robertson, Characterisation of cut and chip behaviour for NR, SBR and BR compounds with an instrumented laboratory device, Plast., Rubber Compos. 48 (1) (2019) 14–23.

[52] S. Futamura, Deformation Index-Concept of hysteretic energy-loss process, Rubber Chem. Technol. 64 (1) (1991) 57–64.

[53] W. Mars, Analysis of stiffness variations in context of strain-, stress-, and energy-controlled processes, Rubber Chem. Technol. 84 (2) (2011) 178–186.

[54] S. Futamura, A.A. Goldstein, Prediction and simulation of tire performance characteristics based on deformation index concept, Rubber Chem. Technol. 89 (1) (2016) 1–21.

[55] B. Huneau, Strain-induced crystallization of natural rubber: a review of X-Ray diffraction investigations, Rubber Chem. Technol. 84 (3) (2011) 425–452.

[56] K. Fujimoto, H. Kofuji, S. Tokui, N. Mifune, Fracture caused by fatigue due to three-dimensional stresses, in: International Rubber Conference, 1986. Kyoto.